AN INVESTIGATION OFMAGNETOHYDRODYNAMIC MAXWELL FLUID FLOW ON ACCELERATING POROUS SURFACE USING SPECTRAL HOMOTOPYANALYSIS METHOD

DADA, M. S.[1], ONWUBUOYA, C.[1], AGUNBIADE, S. A.[1], DISU, A. B.[2]
[1]Faculty of Physical Sciences, Department of Mathematics,
University of Ilorin, Ilorin, Nigeria
[2]Department of Mathematics, Open University of Nigeria, Abuja, Nigeria
E-Mail: dadamsa@gmail.com, onwubuoyacletus@yahoo,
comagunbiade1971@gmail.com, adisu@noun.edu.ng

Abstract
This paper investigates the viscous dissipation Magnetohydrodynamic (MHD) convective flow of Maxwell fluid along a porous accelerating surface in the presence of radiation, buoyancy and heat generation. The Rosseland approximation for optically thick fluid is considered. The physical model is governed by highly nonlinear equations which were transformed using similarity variables and solution technique adopted is Spectral Homotopy Analysis Method (SHAM) which is carried out up to 5^{th} *order of approximation. The influence of pertinent flow parameters on the velocity and temperature are presented both in tabular and graphical forms. A hike in the Eckert number gives a fall in both the velocity and temperature profiles. It is observed that a rise in the Deborah number accelerates the velocity profile but decreases the temperature profile while the magnetic field parameter produces an opposition to the flow. It is found that increasing the radiation parameter produces a significant increase in the thermal condition of the fluid temperature. The numerical results are in better agreement with the existing ones in literature.*

Keywords: Heat Transfer Buoyancy**,** MHD, Spectral Homotopy Analysis Method, Thermal Radiation, Viscous dissipation.

Introduction

Magnetohydrodynamic (MHD) convective, thermal radiation and heat generation/absorption have attracted the interest of many scientists and researchers due to its wide applicability in technological and industrial processes. Most of the industrial fluids such as molten plastics, molten polymers, slurries etc exhibit non-Newtonian properties. Many models has been proposed for the study of the characteristics of non-Newtonian fluid flow. Of the proposed models, Maxwell model is significant because it predicts the relaxation time effects. Ramesh and Gireesha (2014) reported on heat source/sink effects and nano-particles in a stretching surface of a Maxwell fluid in convective boundary conditions. The study concluded that the local Nusselt number is lower while local Sherwood number is more for Maxwell fluids compared to Newtonian fluids. Heat transfer and flow of Maxwell fluid in the presence of thermal conductivity and variable viscosity over a sheet that is exponentially stretched was considered by Singh and Shweta (2013). They solved the momentum and energy equations numerically using an implicit finite-difference scheme and reported that skin friction and heat transfer coefficients are lower for the Maxwell fluid of constant viscosity and thermal conductivity. Riaz and Shabbir (2016) investigated generalized Maxwell fluid flow with new exact solutions. Khan *et al*. (2017) examined Maxwell fluid in a vertically oscillating plate in the presence of heat transfer. Fractional Caputo-Fabrizio derivatives was used for the analysis. Noor *et al*. (2016) analysed influence of heat flux on maxwell fluid in vertically stretched permeable medium plate subject to heat absorption. Their model equations were solved using shooting RK4 method and validated with homotopy-pade solutions. The presence of viscous and

Joule heating dissipation effects which happened to be a part of the motivation for this study are absent in the above Maxwell fluid models

The practical importance of heat generation/absorption, mass transfer and thermal radiation on an accelerating surface is applicable in physical problems such as fluids undergoing exothermic or endothermic chemical reactions. Hence, Chamkha (2000) presented the join effects of buoyancy and thermal radiation on hydromagnetic fluid flow in an accelerating porous surface with sink or heat source. Daniel and Daniel (2015) studied impacts of thermal radiation and bouyancy on MHD fluid flow over a permeable stretching sheet. Homotopy analysis method was applied for the simplification of the problem. Rashidi *et al*. (2014) explored influence of mass and heat transfer in MHD convective flow over a porous stretching sheet with buoyancy and thermal radiation effects. Their computational analysis is done using the homotopy analysis method. Nearly all of the above mentioned investigations are Newtonian types of fluid flow over an accelerating permeable surface. It is hereby of paramount interest of this present study to consider a non-Newtonian maxwell type of flow in the presence of magnetic field, thermal radiation, viscous and Joule heating effect over an accelerating porous surface.

Viscous dissipation in heat transfer plays a significant role in energy source. Viscous dissipation has effects on both the temperature of the fluid flow and heat transfer rates. Alao *et al*. (2016) considered the effects of diffusion-thermo, thermal-diffusion and thermal radiation on an unsteady mass and heat transfer fluid flow with viscous dissipation and chemical reaction through a vertical semi-infinite plate. Spectral relaxation method was used in solving their model equations. Their results showed that an increase in Eckert number speedup the temperature and velocity profiles of the fluid flow. Fagbade *et al*. (2015) examined impact of viscous dissipation, magnetic field and thermophoresis on mixed convection saturated Darcy-Forcheimer fluid flow in a permeable medium. SHAM was used in the computation. They found out that magnetic field can be used to control heat and mass transfer flow characteristics. The investigations discussed above are Newtonian types of fluid in the presence of viscous dissipation. The present study extended the Newtonian model of Daniel and Daniel (2015) to non-Newtonian fluid in order to investigate combined effects of magnetic field, radiation, viscous and Joule heating dissipation on MHD free convective flow of Maxwell fluid over an accelerating permeable surface.

Equations of Motion

A steady two-dimensional boundary layer flow of a viscous incompressible maxwell fluid along a permeable accelerating surface is considered. The physical configuration of the coordinate system (x, y) are shown in figure 1. A magnetic field of uniform strength β_0 is applied in the direction of y-axis. The surface is considered to be permeable and accelerating to allow wall suction/injection with electrically conducting fluid. Magnetic Reynold number is assumed small, such that, the induced magnetic field is negligible. A modified form of the governing equations (Daniel and Daniel, 2015)are;

$$\frac{\partial u}{\partial x} + \frac{\partial v}{\partial y} = 0 \tag{1}$$

$$u\frac{\partial u}{\partial x} + v\frac{\partial u}{\partial y} = \nu\frac{\partial^2 u}{\partial y^2} + g\beta(\vartheta - \vartheta_\infty) - \frac{\sigma\beta_0^2 u}{\rho} - \lambda\left(u^2\frac{\partial^2 u}{\partial x^2} + v^2\frac{\partial^2 u}{\partial y^2} + 2uv\frac{\partial^2 u}{\partial x\,\partial y}\right) \tag{2}$$

$$u\frac{\partial \vartheta}{\partial x} + v\frac{\partial \vartheta}{\partial y} = \alpha\frac{\partial^2 \vartheta}{\partial y^2} - \frac{1}{\rho c_p}\frac{\partial q_r}{\partial y} + \frac{\mu}{\rho c_p}\left(\frac{\partial u}{\partial y}\right)^2 + \frac{Q_0}{\rho c_p}(\vartheta - \vartheta_\infty) + \frac{\sigma\beta_0^2}{\rho c_p}u^2 + \frac{\beta^* u}{\rho c_p}(\vartheta_\infty - \vartheta). \tag{3}$$

subject to the conditions

$$u = U_w(x) = ax; v = v_0; \vartheta = \vartheta_w = \vartheta_\infty + A_0 x \quad at \quad y = 0 \tag{4}$$

$$u \to 0, \vartheta \to \vartheta_\infty, \text{ as } \quad y = \infty \tag{5}$$

where u and v are the velocity components in x and y direction respectively, ν is the kinematic viscosity, g is the acceleration due to gravity, β is the thermal expansion coefficient, ϑ is the temperature of the fluid, ϑ_∞ is the free stream temperature, σ is the electric conductivity, ρ is the fluid density, β_0 is the magnetic field strength, λ is the relaxation time, α is the thermal conductivity, c_p is the specific heat at constant pressure, μ is the dynamic viscosity, Q_0 is the heat generation or absorption, q_r is the radiative heat flux, a is the stretching rate (constant), v_0 is the wall suction velocity when $v_0 > 0$ or injection when $v_0 < 0$ and ϑ_w is the wall temperature.

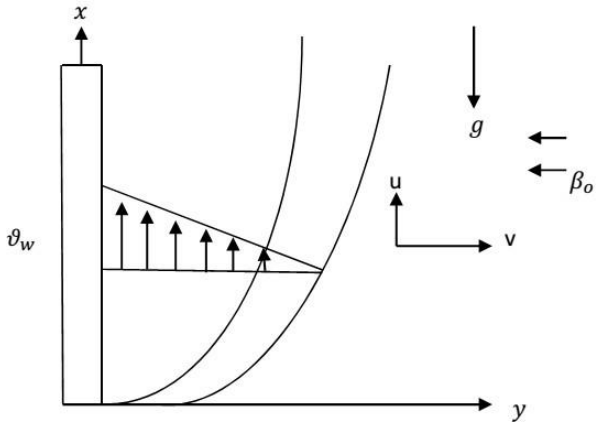

Figure 1: Physical Configuration of the Model

Using the Rosseland approximation for the radiative heat flux q_r and the similarity transformation

$$\eta = \sqrt{\frac{a}{\nu}}y, \ \psi(x,y) = \sqrt{a\nu}xf(\eta), \ \theta = \frac{\vartheta - \vartheta_\infty}{\vartheta_w - \vartheta_\infty} \tag{6}$$

and

$$u = \frac{\partial \psi}{\partial y}, \ v = -\frac{\partial \psi}{\partial x}$$

as properties of the stream function ψ, the governing equations (2) and (3) are transformed to

$$\frac{d^3f}{d\eta^3} + f\frac{d^2f}{d\eta^2} - \left(\frac{df}{d\eta}\right)^2 + Gr\theta - Mg\frac{df}{d\eta} - \beta\left(f^2\frac{d^3f}{d\eta^3} - 2\frac{df}{d\eta}f\frac{d^2f}{d\eta^2}\right) = 0 \tag{7}$$

$$\left(\frac{1+Rp}{Pr}\right)\frac{d^2\theta}{d\eta^2} + f\frac{d\theta}{d\eta} - \theta\frac{df}{d\eta} + E_0\left(\frac{d^2f}{d\eta^2}\right)^2 + E_0Mg\left(\frac{df}{d\eta}\right)^2 + \gamma\theta - Q\frac{df}{d\eta}\theta = 0 \tag{8}$$

subject to:

$$\frac{df}{d\eta}(0) = 1, \ f(0) = -\alpha_0, \ \theta(0) = 1 \qquad at\eta = 0 \tag{9}$$

$$\frac{df}{d\eta}(\infty) = 0, \qquad \theta(\infty) = 0 \qquad as\eta \to \infty \tag{10}$$

where $Gr = \frac{g\beta(\vartheta_w - \vartheta_\infty)}{a^2x}$ is the Grashof number, $Mg = \frac{\sigma\beta_0^2}{a\rho}$ is the magnetic parameter, $\beta = a\lambda$ is the Deborah number, $Rp = \frac{16\sigma^*\vartheta_\infty^3}{3k^*k}$ is the thermal radiation parameter, $Pr = \frac{\nu}{\alpha}$ is the Prandlt number, $E_0 = \frac{(ax)^2}{c_p(\vartheta_w - \vartheta_\infty)}$ is the Eckert number, $\gamma = \frac{Q_0}{\rho c_p a}$ is the heat source/sink parameter, $Q =$

$\frac{\beta^* x}{\rho c_p}$ is the internal heat generation/absorption coefficient parameter, $\alpha_0 = \frac{v_w}{(av)^{\frac{1}{2}}}$ is the suction or injection. The physical quantities of engineering interest are the local skin friction (Cf) and Nusselt number (Nu) respectively defined as:

$$C_f = \frac{\tau_w}{\eta_0\left(\sqrt{\frac{a}{\nu}}\right)ax} \tag{11}$$

$$Nu = \frac{\nu q_w}{\alpha a(\vartheta_w - \vartheta_\infty)} \tag{12}$$

With reference to the Maxwell fluid, radiative transfer equation and the Rosseland approximation, we have the wall shear stress (τ_w) and the rate of heat transfer (q_w) written as:

$$\tau_w = \eta_0 \frac{\partial u}{\partial y} - \lambda\left[2uv\frac{\partial u}{\partial x} + v^2\frac{\partial u}{\partial y}\right]_{\eta=0} \tag{13}$$

$$q_w = -\alpha\left(\frac{\partial \vartheta}{\partial y}\right)_{\eta=0} - \frac{4\sigma^*}{3k^*}\left(\frac{\partial \vartheta^4}{\partial y}\right)_{\eta=0} \tag{14}$$

Using (6), equations (11) and (12) become

$$Re_x^{\frac{1}{2}} C_f = \frac{d^2 f}{d\eta^2} + \beta\left[2(\frac{df}{d\eta})^2 f - f^2\frac{d^2 f}{d\eta^2}\right]_{\eta=0}, \quad \frac{Nu}{Re_x^{\frac{1}{2}}} = -\frac{d\theta}{d\eta}|_{\eta=0} + Rp\frac{d^2\theta}{d\eta^2}|_{\eta=0} \tag{15}$$

where $Re_x^{\frac{1}{2}}$ is the local Reynolds number and it defined as $Re_x^{\frac{1}{2}} = \frac{ax^2}{\nu}$

The Skin friction and the Nusselt number are useful from an engineering point of view due to the fact that frictional drag exerted and the rate of heat transfer on the surface affect the fluid flow.

Spectral homotopy analysis method (SHAM)

SHAM is the numerical version of the well known Homotopy Analysis Method (HAM). It combines the Chebyshev spectral collocation method with HAM in solving ordinary differential equations (Trefethen, 2000). The interval [0,∞) with open upper limit is transformed into the region [-1,1] by applying the domain truncation method applicable to the boundary value problem and solve within the region [0, L] in place of [0, ∞), where L is the scaling parameter. Also, the boundary conditions of the governing equations are make homogeneous by introducing the following transformations

$$\zeta = \frac{2\eta}{L} - 1, \qquad \zeta \in [-1,1] \tag{16}$$

$$f(\eta) = f(\zeta) + f_0(\eta) \tag{17}$$

$$\theta(\eta) = \theta(\zeta) + \theta_0(\eta) \tag{18}$$

where $f_0(\eta)$ and $\theta_0(\eta)$ are the initial approximations that are chosen to satisfy the governing boundary conditions. Substituting (17) and (18) into (7) and (8), we have

$$f'''(\zeta) + f(\zeta)f''(\zeta) + a_1 f(\zeta) + a_2 f''(\zeta) - f'(\zeta)f'(\zeta) + a_3 f'(\zeta) + Gr\theta(\zeta) - Mgf'(\zeta) - \tag{19}$$

$$\beta f(\zeta)f(\zeta)f'''(\zeta) + a_4 f(\zeta)f(\zeta) + a_5 f(\zeta)f'''(\zeta) + a_6 f(\zeta) + a_7 f'''(\zeta) + 2\beta f'(\zeta)f(\zeta)f'''(\zeta)$$

$$+a_8 f'(\zeta)f(\zeta) + a_9 f'(\zeta)f'''(\zeta) + a_{10} f'(\zeta) + a_{11} f(\zeta)f'''(\zeta) + a_{12} f(\zeta) + a_{13} f'''(\zeta) = H_1(\eta)$$

$$\left(\frac{1+Rp}{Pr}\right)\theta''(\zeta) + f(\zeta)\theta'(\zeta) + b_1 f(\zeta) + b_2\theta'(\zeta) - \theta(\zeta)f'(\zeta) + b_3\theta(\zeta) + b_4 f'(\zeta) + \tag{20}$$

$$E_0 f''(\zeta)f''(\zeta) + b_5 f''(\zeta) + E_0 Mgf'(\zeta)f'(\zeta) +$$

$$b_6 f'(\zeta) + \gamma\theta(\zeta) + b_8\theta(\zeta) - Qf'(\zeta)\theta(\zeta) + b_7 f'(\zeta) = H_2(\eta)$$

subject to:

$$f(-1) = f'(-1) = f'(1) = 0, \qquad \theta(-1) = \theta(1) = 0 \tag{21}$$

where the primes in the equations above denoted differentiation with respect to ζ and setting

$$a_1 = f''_0(\eta),\ a_2 = f_0(\eta),\ a_3 = -2f'_0(\eta),\ a_4 = -\beta f'''_0,\ a_5 = -2\beta f_0(\eta),\ a_6 = -2\beta f_0(\eta),$$

$$a_7 = -\beta f_0^2(\eta), a_8 = 2\beta f'''_0(\eta),\ a_9 = 2\beta f_0(\eta),\ a_{10} = 2\beta f_0(\eta),$$

$$a_{11} = 2\beta f'_0(\eta),\ a_{12} = 2\beta f'_0(\eta) f'''_0(\eta),\ a_{13} = 2\beta f'_0(\eta) f_0(\eta)$$

$$H_1(\eta) = -f'''_0(\eta) - f_0(\eta) f''_0(\eta) + f'_0(\eta) f'_0(\eta) - Gr\theta_0(\eta) + Mgf'_0(\eta) + \beta f_0^2(\eta) f'''_0(\eta)$$

$$-2\beta f'_0(\eta) f_0(\eta) f'''_0(\eta)$$

$$b_1 = \theta'_0(\eta),\ b_2 = f_0(\eta),\ b_3 = -f'_0(\eta),\ b_4 = -\theta_0(\eta),\ b_5 = 2E_0 f''_0(\eta),$$

$$b_6 = 2E_0 Mgf'_0(\eta), b_7 = -Q\theta_0(\eta),\ b_8 = -Qf'_0(\eta)$$

$$H_2(\eta) = -\left(\tfrac{1+Rp}{Pr}\right)\theta''_0(\eta) - f_0(\eta)\theta'_0(\eta) + \theta_0(\eta) f'_0(\eta) - f''^2_0(\eta) - E_0 Mgf'^2_0(\eta) -$$

$$\gamma\theta_0(\eta) + Qf'_0(\eta)\theta_0(\eta)$$

From (19) and (20), the non-homogeneous linear part is given by

$$f'''_l + a_1 f_l + a_2 f''_l + a_3 f'_l + Gr\theta_l - Mgf'_l + a_6 f_l + a_7 f'''_l + a_{10} f'_l + a_{12} f_l + a_{13} f'''_l = H_1(\eta) \tag{22}$$

$$\left(\tfrac{1+Rp}{Pr}\right)\theta''_l + b_1 f_l + b_2\theta'_l + b_3\theta_l + b_4 f'_l + b_5 f''_l + b_6 f'_l + \gamma\theta_l + b_8\theta_l + b_7 f'_l = H_2(\theta) \tag{23}$$

subject to

$$f'_l(-1) = f'_l(1) = 0,\ f_l(-1) = f_l(1) = 0,\ \theta_l(-1) = \theta_l(1) = 0 \tag{24}$$

The next thing is to use the Chebyshev pseudospectral method to solve (22) and (23). Approximate the unknown functions $f_l(\zeta)$ and $\theta_l(\zeta)$ as a truncated series of Chebyshev polynomials of the form

$$f_l(\zeta) \neg f_l^N = \sum_{k=0}^{N} f_k^N \vartheta_{1k}(\zeta_J), \qquad J = 0,1,2,\ldots,N \tag{25}$$

$$\theta_l(\zeta) \neg \theta_l^N = \sum_{k=0}^{N} \theta_k^N \vartheta_{2k}(\zeta_J), \qquad J = 0,1,2,\ldots,N \tag{26}$$

where k^{th} Chebyshev polynomials are ϑ_{1k} and ϑ_{2k} with the associated coefficients f_k, θ_k and $\zeta_0, \zeta_1, \zeta_2, \ldots, \zeta_N$ are Gauss-Lobatto collocation point defined by

$$\zeta_J = \cos(\tfrac{\pi J}{N}) \qquad J = 0,1,2,\ldots,N \tag{27}$$

In (27), N is the number of collocation points. At this collocation points, the derivatives of the function $f_l(\zeta), \theta_l(\zeta)$ are presented as;

$$\frac{d^r f_l}{d\zeta^r} = \sum_{k=0}^{N} D_{kJ}^r f_l(\zeta_J), \qquad \frac{d^r \theta_l}{d\zeta^r} = \sum_{k=0}^{N} D_{kJ}^r \theta_l(\zeta_J) \tag{28}$$

where r is the order of differentiation and $D = \frac{2}{L}$D and D is the Chebyshev spectral differentiation matrix. Applying (25)-(28) into (22) and (23), we obtain

$$AF_L = G \tag{29}$$

subject to the boundary conditions

$$f_l(\zeta_N) = -\alpha_0, \qquad \sum_{k=0}^{N} D_{Nk} f_k(\zeta_k) = 1, \sum_{k=0}^{N} D_{0k} f_k(\zeta_k) = 0, \qquad \theta_l(\zeta_N) = 1, \quad \theta_l(\zeta_0) = 0, \tag{30}$$

where

$$A = \begin{bmatrix} A_{11} A_{12} \\ A_{12} A_{22} \end{bmatrix}$$

and

$$A_{11} = D^3 + a_1 + a_2 D^2 + a_3 D - MgD + a_6 + a_7 D^3 + a_{10} D + a_{12} D + a_{13} D^3,\ A_{12} = GrI,$$

$$A_{21} = b_1 + b_4 D + b_5 D^2 + b_6 D + b_7 D,\ A_{22} = \left(\frac{1+Rp}{Pr}\right) D^2 + b_2 D + b_3 + \gamma + b_8 I$$

$$F_l = [f_l(\zeta_0), \ldots, f_l(\zeta_N), \theta_l(\zeta_0), \ldots, \theta_l(\zeta_N)], G = [H_l(\eta_0), \ldots, H_l(\eta_N), H_2(\eta_0), \ldots, H_2(\eta_N)]$$

$$a_i = diag([a_i(\eta_0), \ldots, a_i(\eta_{N-1}), a_i(\eta_{N-1}, a_i(\eta_N]),;$$

$$b_i = diag([b_i(\eta_0), \ldots, b_i(\eta_{N-1}), b_i(\eta_{N-1}, b_i(\eta_N]) \qquad i = 1,2,3$$

In other to implement the boundary conditions (30), the first and the last rows of A are deleted. The boundary conditions are then imposed on the modified matrix A. Now setting the modified matrix G to zero of $f_l(\zeta_0), \ldots, f_l(\zeta_N), \theta_l(\zeta_0), \ldots, \theta_l(\zeta_N)$ are determined from

$$F_l = A^{-1} G, A \neq 0 \tag{31}$$

Equation (31) with the initial approximation are the SHAM solution of the governing equations. The following linear operators are defined in order to seek for the convergent series of SHAM approximation solutions of (19) and (20)

$$L_f[\bar{f}(\eta, q), \bar{\theta}(\eta, q)] = f'''_l + a_1 f_l + a_2 f''_l + a_3 f'_l + Gr\theta_l - Mgf'_l + a_6 f_l + a_7 f'''_l + a_{10} f'_l + a_{12} f_l + a_{13} f'''_l \tag{32}$$

$$L_\theta[\bar{f}(\eta, q), \bar{\theta}(\eta, q)] = \left(\frac{1+Rp}{Pr}\right)\theta''_l + b_1 f_l + b_2 \theta'_l + b_3 \theta_l + b_4 f'_l + b_5 f''_l + b_6 f'_l + \gamma\theta_l \tag{33}$$

where $q \in [0,1]$ is the embedding parameter and $\bar{f}(\eta, q), \bar{\theta}(\eta, q)$ are the unknown functions. We have the zeroth order deformation equation given by:

$$(1-q)L_f[\bar{f}(\eta; q) - f_l(\xi)] = q\hbar_f N_f[\bar{f}(\eta; q), \bar{\theta}(\eta, q)] - H_1(\eta), \tag{34}$$

$$(1-q)L_\theta[\bar{\theta}(\eta; q) - \theta_l(\xi)] = q\hbar_\theta N_\theta[\bar{f}(\eta; q), \bar{\theta}(\eta, q)] - H_2(\eta) \tag{35}$$

where $\hbar_f, \hbar_\theta$ are nonzero convergence controlling auxiliary parameter, $N_{\bar{f}}$ and $N_{\bar{\theta}}$ are nonlinear operations given by:

$$N_f[\bar{f}(\eta, q), \bar{\theta}(\eta, q)] = ff'' - f'^2 - \beta f^2 f''' + a_4 f^2 + a_5 ff''' + 2\beta f' ff''' + a_8 f' f + a_9 f' f''' + a_{11} ff''' \tag{36}$$

$$N_\theta[\bar{f}(\eta, q), \bar{\theta}(\eta, q)] = f\theta' - \theta f' + E_0 f''^2 + E_0 Mgf'^2 \tag{37}$$

Equations (34) and (35) are differentiated m −times with respect to q and making q to be equals zero, the mth order deformation equations becomes

$$L_f[f_m(\xi) - \chi_m f_{m-1}(\xi)] = \hbar_f R_m^f, \tag{38}$$

$$L_\theta[\theta_m(\xi) - \chi_m \theta_{m-1}(\xi)] = \hbar_\theta R_m^\theta \tag{39}$$

subject to

$$f_m(-1) = f'_m(-1) = f'_m(1) = 0, \tag{40}$$

$$\theta_m(-1) = \theta_m(1) = 0. \tag{41}$$

where

$$R_m^f(\xi) = f'''_{m-1} + a_1 f_{m-1} + a_2 f''_{m-1} + a_3 f'_{m-1} + Gr\theta_{m-1} - Mgf'_{m-1} + a_6 f_{m-1} + a_7 f'''_{m-1} + a_{10} f'_{m-1} + a_{12} f_{m-1} +$$

$$a_{13} f'''_{m-1} + \sum_{n=0}^{m-1} (f_n f_{m-1-n} - f'_n f'_{m-1-n} - \beta f_n^2 f'''_{m-1-n} + a_4 f_n f_{m-1-n} + a_5 f_n f'''_{m-1-n} +$$

$a_8 f'_n f_{m-1-n} + a_9 f'_n f'''_{m-1-n}) + \sum_{i=0}^{n} \sum_{n=0}^{m-1} (2\beta f_i f'_{n-i} f'''_{m-1-n}) - H_1(\eta)(1-\chi_m)$ (42)

$$R_m^{\theta}(\xi) = \left(\frac{1+Rp}{Pr}\right)\theta''_{m-1} + b_1 f_{m-1} + b_2 \theta'_{m-1} + b_3 \theta_{m-1} + b_4 f'_{m-1} + b_5 f''_{m-1} + b_6 f'_{m-1} + \gamma\theta_{m-1} + b_7 f'_m - + b_8 \theta_{m-1} \sum_{n=0}^{m-1} (f_n \theta'_{m-1-n} - \theta_n f'_{m-1-n} + E_0 f''_n f''_{m-1-n} + E_0 M g f'_n f'_{m-1-n}) - H_2(\eta)(1-\chi_m)$$ (43)

Upon the application of Chebyshev pseudo-spectral transformation on (38)-(43) gives

$$Af_m = (\chi_m + \hbar)Af_{m-1} - \hbar(1-\chi_m)G + \hbar Q_{m-1}$$ (44)

subject to the following boundary conditions

$$f_m(\xi_N) = 0, \qquad f_m(\xi_0) = 0,$$ (45)

$$\theta_m(\xi_N) = 0, \qquad , \theta_m(\xi_0) = 0.$$ (46)

where $F_m = [f_m(\xi_0), f_m(\xi_1), \ldots, f_m(\xi_N), \theta_m(\xi_0), \theta_m(\xi_1), \ldots, \theta_m(\xi_N)]^T$ and

$$Q_{1,m-1} = \sum_{n=0}^{m-1} (f_n)(f_{m-1-n}) - (Df_n)(Df_{m-1-n}) + (a_4 f_n) + (a_5 f_n)(D^3 f_{m-1-n}) + (a_5 D f_n)(f_{m-1-n})$$

$$+(a_9 D f_n)(D^3 f_{m-1-n}) + \sum_{i=0}^{n} \sum_{n=0}^{m-1} [(2\beta f_i D f_{n-i})(D^3 f_{m-1-n}) - (\beta f_i f_{n-i})(D^3 f_{m-1-n})]$$ (47)

$$Q_{2,m-1} = \sum_{n=0}^{m-1} [(f_n)(D\theta_{m-1-n}) - (\theta_n)(Df_{m-1-n}) + (E_0 D^2 f_n)(D^2 f_{m-1-n}) + (E_0 M g D f_n)(Df_{m-1-n})]$$ (48)

Using (44), the following recursive formula are obtained for $m \geq 1$

$$F_m = (\chi_m + \hbar)A^{-1}.\bar{A}f_{m-1} + \hbar A^{-1}[Q_{m-1} - (1+\chi_m)G],$$ (49)

$$\Theta_m = (\chi_m + \hbar)A^{-1}.\bar{A}\theta_{m-1} + \hbar A^{-1}[Q_{m-1} - (1+\chi_m)G]$$ (50)

The initial approximation can be obtained from (31). Starting from this initial approximation, higher order approximations $F_m(\xi)$ and $\Theta_m(\xi)$ from $m \geq 1$ can be obtained from (49) and (50).

Result and Discussions

Equations (7) and (8) subject to (9) and (10) has been solved numerically using SHAM with their governing parameters: Grashof number (Gr), magnetic parameter (Mg), Deborah number (β), radiation parameter (Rp), Prandtl number Pr, Eckert number (E_0), heat source/sink (γ) and suction velocity (α_0). SHAM combines the idea of Chebyshev pseudo-spectral method with HAM. For the numerical analysis, the following values are used for the controlling parameters: $Pr = 0.71, Gr = 2.0, Mg = 0.5, \beta = 0.01, Rp = 0.5, E_0 = 0.01, \gamma = 0.1, \alpha_0 = -0.5$. Hence, in all our computations we utilized the above values unless otherwise stated.

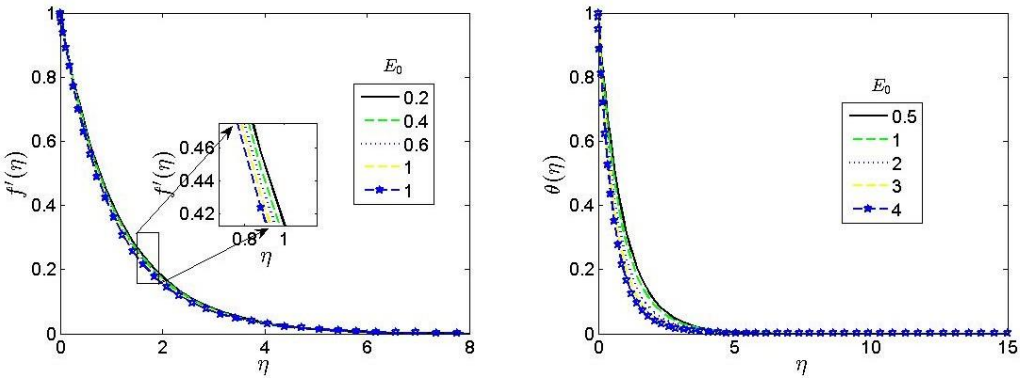

Figure 2: Effect of E_0 on the velocity and temperature profiles

Figure 2 illustrates the effects of Eckert number on the velocity and temperature profiles. Viscous dissipation influences both the temperature and heat transfer rates. It is expected that the Eckert number hike the velocity and temperature profiles as a result of greater viscous dissipative heat. The presence of Joule heating dissipation reduces the viscous dissipative heat and thereby result to a fall in both the velocity and temperature profiles as shown in Figure 2.

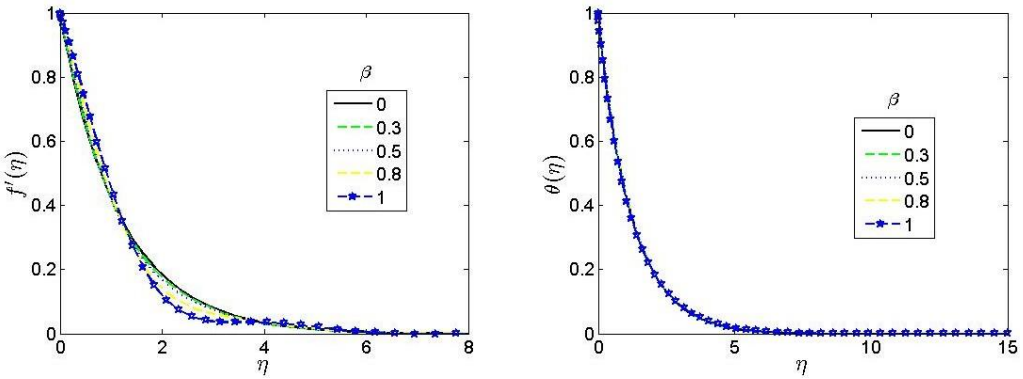

Figure 3: Effect of β on the velocity and temperature profiles

Figure 3 depicts the effect of the Deborah number on the velocity and temperature profiles. It is observed that as the Deborah number increases, the velocity increases near the boundary layer while the temperature profile slightly decreases. This implies that the Deborah number has the tendency of increasing the boundary layer thickness.

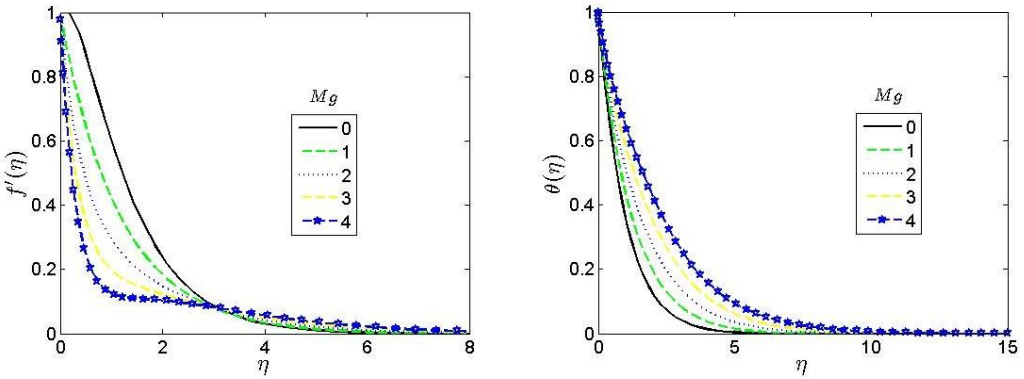

Figure 4: Effect of Mg on the velocity and temperature profiles

The effect of magnetic parameter Mg on the velocity and temperature profiles is displayed in Figure 4. A noticeable decrease near the boundary layer in the velocity profile and increase in the temperature profile is observed with a rise in magnetic parameter. The application of transversely magnetic field to the flow invokes lorentz force thereby producing an opposition to the flow of the the fluid and enhancement of the temperature profile.

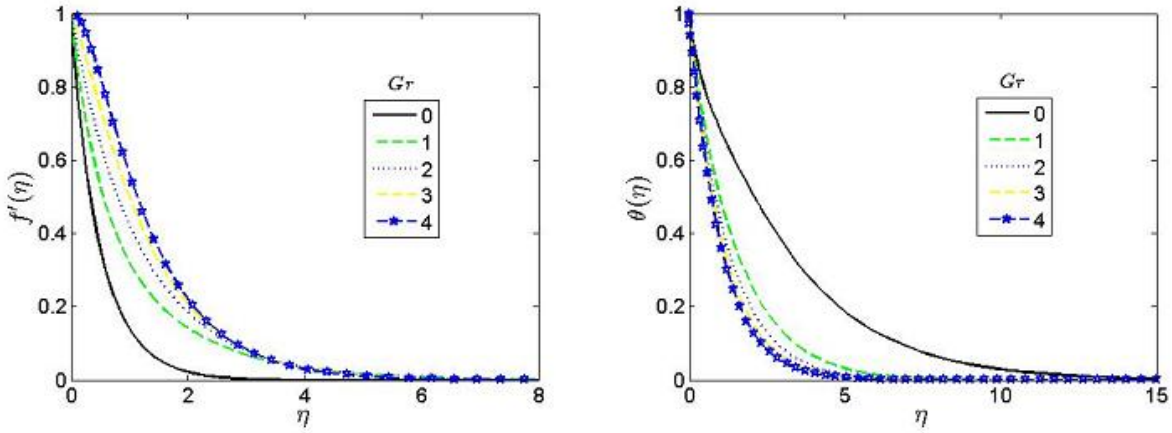

Figure 5: Effect of Gr on the velocity and temperature profiles

The effect of the Grashof number (Gr) on the velocity and temperature profiles is illustrated in Figure 5. Gr is a dimensionless number which estimates the ratio of the buoyancy to viscous force acting on a fluid. It is noticed that increasing the Grashof number add more thermal energy into the fluid molecules and loosen up intermolecular forces within the fluid particles.Thus, it increases the velocity profile as shown in Figure 5. Also, increasing the Grashof number the fluid particle gathered more momentum and lost additional heat to the surrounding, thus decreases the temperature profile as depicted in Figure 5.

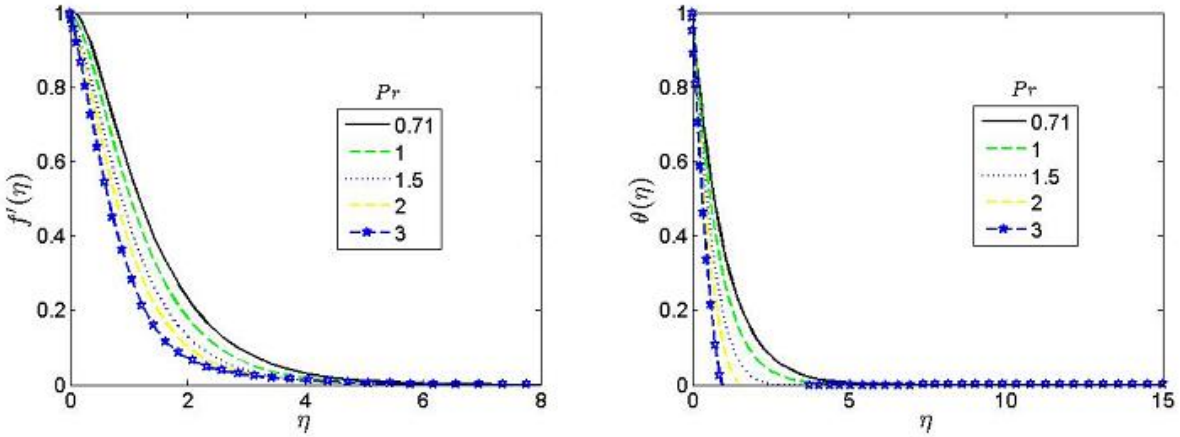

Figure 6: Effect of Pr on the velocity and temperature profiles

Figure 6 displays the effect of Prandtl number on the flow profile. The Prandtl number approximates the ratio of the momentum diffusion to thermal diffusion. From Figure 6, as the Prandtl number increases, the velocity as well as the temperature profile decreases. This is because increasing the Prandtl number decreases the thermal diffusion and makes the thermal boundary layer to become thinner. On the hand, fluids with higher Prandtl number possesses more viscosities.

In other to show the correctness of the code used in the present study, we compare the computed results with Daniel and Daniel (2015) and Chamkha (2000) in the absence of parameters such as Deborah number, thermal radiation and viscous dissipation in Table 1. Our model is the general form of Daniel and Daniel (2015) when pertinent parameters $\beta = E_0 = 0$. The result shown in

table 1 indicates that the present results with SHAM is in good agreement with the results of Daniel and Daniel (2015) and Chamkha (2000). Table 2 illustrates the influence of Deborah number (β) and Eckert number (E_0) on the skin friction coefficient and Nusselt number respectively when $Pr = 0.71, Gr = 2.0, Mg = 0.5, \beta = 0.01, Rp = 0.5, \gamma = 0.1, \alpha_0 = -0.5, h_f = h_\theta = h_\phi = -0.5$. It is observed that a hike in both Deborah and Eckert number gives rise to both skin friction and Nusselt number.

Table 1: Comparison of computational values of wall temperature gradient $(-\theta'(0))$ with Daniel and Daniel (2015) and Chamkha (2000)

	$\beta_0 = 0.45$ $Q = 0.5$	$\beta_0 = 0.45$ $Q = 1.0$	$\beta_0 = 0$ $Q = 0.5$	$\beta_0 = 0$ $Q = 1.0$	$\beta_0 = -1.5$ $Q = 0.5$	$\beta_0 = -1.5$ $Q = 1.0$
SHAM	0.82348	0.96193	0.94777	1.07896	1.57088	1.66192
HAM	0.82396	0.96190	0.94765	1.07895	1.57077	1.66182
Implicit FDM	0.82397	0.96191	0.94769	1.07996	1.57077	1.66184

Table 2: Numerical values of the local skin friction and local Nusselt number for different values of Deborah number (β) and Eckert number (E_0)

β	E_0	$-f''(0)$	$-\theta(0)$
0.0	0.2	0.88530	0.89896
	0.4	0.91423	0.94909
	0.6	0.94067	0.99697
0.5	0.2	0.88354	0.89894
	0.4	0.91252	0.94907
	0.6	0.93900	0.99693

Conclusion

In this paper, we have employed the discrete version of HAM namely SHAM in solving the transformed (11) and (12) subject to (13). The procedure on how to apply the SHAM is discussed extensively in section 3. Numerical simulations were done and it is found that increasing the magnetic parameter (Mg) decreases the velocity profile and increases the temperature profile which accounts for the presence of a drag force known as Lorentz force that opposes the fluid transport. A hike in the Deborah number increases the velocity near the boundary but decreases the temperature profile. Also, arise in the Prandtl number leads to a decrease in both the velocity and temperature profiles respectively. From the heated surface, at higher Prandtl, heat diffuses away more rapidly. These results are applicable in controlling cooling rate, for instance, in engine coolant production.

References

Alao, F. I., Fagbade, A. I., & Falodun, B. O. (2016). Effects of thermal radiation, Soret and Dufour on an unsteady heat and mass transfer flow of a chemically reacting fluid past a semi-infnite vertical plate with viscous dissipation, *Journal of the Nigerian Mathematical Society, 35,* 142-158.

Chamkha, A. J. (2000). Thermal radiation and buoyancy effects on hydromagnetic flow over an accelerating permeable surface with heat source or sink. *International Journal of Engineering Science, 38*(15),1699-1712.

Daniel, Y. S., & Daniel, S. K. (2015). Studied effects of buoyancy and thermal radiation on MHDflow over a stretching porous sheet using homotopy analysis method. *Alexandria Engineering Journal 54,* 705-712.

Fagbade, A. I., Falodun, B. O., & Boneze, C. U. (2015). Influence of Magnetic Field, Viscous Dissipation and Thermophoresis on Darcy-Forcheimer Mixed Convection Flow in Fluid Saturated Porous Media, *American Journal of Computational Mathematics, 5,* 18-40.

Khan, I. K., Nehad, A. S., Muhsud, Y. & Vieru, D. (2017). Heat transfer analysis in a Maxwell fluid over an oscillating vertical plate using fractional Caputo-Fabrizio derivatives. *European Physical Journal Plus.,* 132, 194-206. http://doi:10.1140/epjp/i2017-11456-2.

Noor, N. F. M., Rizwan, U. l., Haq, A. S., & Hashim, I. (2016). Heat flux performance in a porous medium embedded Maxwell fluid flow over a vertically stretched plate due to heat absorption, *Journal of Nonlinear Science and Applications, 9*, 2986-3001.

Ramesh, G. K. and Gireesha, B. J. (2014). Influence of heat source/sink on a Maxwell fluid over a stretching surface with convective boundary condition in the presence of nanoparticles. *Ain Shams Engineering Journal, 5*, 991-998.

Rashidi, M. M., Rostami, B., Freidoonimehr, N. & Abbasbandy, S. (2014). Free convective heat and mass transfer for MHD fluid flow over a permeable vertical stretching sheet in the presence of the radiation and buoyancy effects, *Ain Shams Engineering Journal,* 5, 901-912.

Riaz, M. B., & Shabbir, M. A. (2016). New exact solutions for the flow of generalized Maxwell fluid. *Journal of computational and theoretical nanoscience, 13*(18), 5254-5257.

Singh, V. & Shweta, A. (2013). Flow and heat transfer of Maxwell fluid with variable viscosity and thermal conductivity over an exponentially stretching sheet. American *Journal of Fluid Dynamics. 3*(4), 87-95.

Trefethen, L. N. (2000). *Spectral Methods in MATLAB*, SIAM, 2000.